CONF-8606157--2

MASTER

CONF-8606157--2

DE86 014232

MAYER-FERMI THEORY AND THE LONG SEQUENCES IN THE PERIODIC TABLE

D. C. Griffin

Department of Physics, Rollins College
Winter Park, Florida 32789
and Physics Division, Oak Ridge National Laboratory
Oak Ridge, Tennessee 37831

Robert D. Cowan

Los Alamos National Laboratory
Los Alamos, New Mexico 87545

M. S. Pindzola

Department of Physics, Auburn University
Auburn, Alabama 36849
and Physics Division, Oak Ridge National Laboratory
Oak Ridge, Tennessee 37831

INTRODUCTION

58 years ago, Fermi[1] employed the Thomas-Fermi (TF) statistical model of the atom to predict a collapse of the 4f orbital for atomic numbers between 55 and 60, and thereby explained the formation of the first rare-earth series of elements. In 1941, Maria Mayer[2] used the same model to predict the onset of a second rare-earth series with the orbital collapse of the 5f electron for atomic numbers between 86 and 91. She also showed that the abrupt changes in the character of these electrons can be explained in terms of the f-electron effective potential which, in these regions of the periodic table, consists of two wells separated by a positive centrifugal barrier.

Since Mayer's classical paper, the results of a number of more complete calculations using the Thomas-Fermi-Dirac (TFD) model,[3] as well as the self-consistent Hartree-Fock-Slater,[4] Hartree plus statistical exchange scheme (HX)[5] and Hartree-Fock (HF)[6] methods have been employed to study the variation of d-, f- and even g-electron wave functions within the excited states of neutral atoms. In the next section of this paper, we employ the results of the more recent self-consistent-field calculations to consider the now well known changes in radial wave functions for d electrons which occur preceding the onset of the transition series of elements, and for f electrons preceding the onset of the lanthanide and actinide series. The sensitivity of the radial wave functions to variations in the effective potential is discussed, and the large variation of the radial wave functions between the LS terms of

By acceptance of this article, the publisher or recipient acknowledges the U. S. Government's right to retain a nonexclusive, royalty - free license in and to any copyright covering the article.

DISTRIBUTION OF THIS DOCUMENT IS UNLIMITED

certain types of excited configurations in these regions of the periodic system is analyzed.

The changes in the d- and f-radial wave functions along isoelectronic and isonuclear sequences are much more gradual than the sudden contractions of the wave functions that occur within neutral atomic species. Nevertheless, such variations may lead to large term-dependent effects in certain excited configurations which are important in electron-impact excitation, as well as photoabsorption. The excitation of inner-shell electrons followed by autoionization can in some cases dominate electron-impact ionization cross sections.[7,8,9] This is especially true in species with intermediate to heavy atomic mass where term-dependent effects may also be important. In the third section of this paper, several examples of electron-impact ionization, where the indirect mechanism is dominant and term dependence significantly affects the excitation of the inner-shell electron, are explained by analyzing the effective potentials for the excited electrons in the intermediate autoionizing states.

Finally, potential barriers can lead to significant term-dependent effects in the continuum which play an important role, not only in photoionization, but also direct electron-impact ionization. In the fourth section, we consider several examples where such effects are essential to the accurate determination of both single and double electron-impact ionization cross sections.

THE DOUBLE-WELL EFFECTIVE POTENTIAL AND WAVE FUNCTION COLLAPSE

Near the beginning of the rare-earth series of elements the excited f electrons undergo abrupt changes in binding energy. This is shown graphically in Fig. 1 in terms of the effective quantum number n^*, which

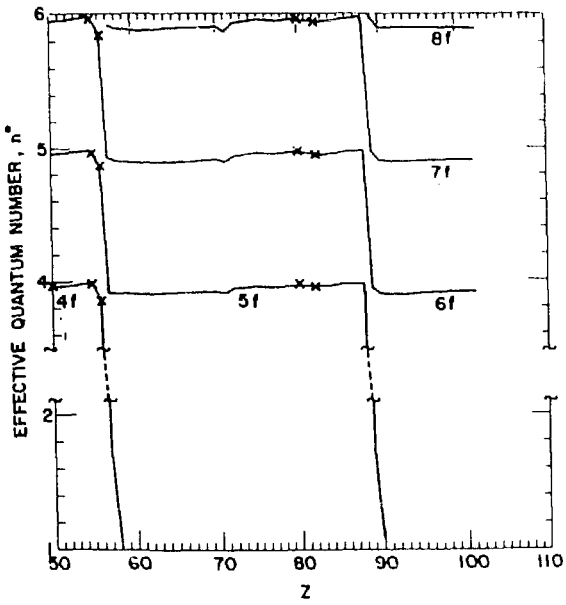

Fig. 1. Effective quantum numbers for f electrons as a function of atomic number from Ref. 5. Curves, theoretical values calculated using HX binding energies; x, experimental values.

for neutral atoms is defined by the equation:

$$n^* = E_B^{-1/2} , \tag{1}$$

where E_B is the binding energy of the electron in rydbergs. These sudden changes are accompanied by a corresponding change in the nature of the f electrons consisting of contractions of the wave functions to smaller radii. In order to understand these effects it is useful to introduce an effective central potential, so that the radial differential equation can be written as:

$$\left[-\frac{d^2}{dr^2} + V_{eff}(r) \right] P_{n\ell}(r) = E_{n\ell} P_{n\ell}(r) , \tag{2}$$

where the effective potential, $V_{eff}(r)$, and the eigenvalue, $E_{n\ell}$, are in rydberg units. If one employs the Hartree-Fock method, $V_{eff}(r)$ is defined by the equation:

$$V_{eff}(r) = \frac{\ell(\ell+1)}{r^2} - \frac{2Z}{r} + \frac{2Y(n\ell;r)}{r} + \frac{2X(n\ell;r)}{rP_{n\ell}(r)} + \sum_{n'} \frac{E_{n\ell,n'\ell}\, P_{n'\ell}(r)}{P_{n\ell}(r)} , \tag{3}$$

where we use a notation similar to Fischer's.[10] In Eq. (3), Z is the atomic number; $2Y(n\ell;r)/r$ is simply the direct potential when the subshell is singly occupied, as it is for the cases of interest here; $2X(n\ell;r)/r$ is the exchange function; and $E_{n\ell,n'\ell}$ is a Lagrangian multiplier used to force orthogonality between radial wave functions with equal values of ℓ but different n. This function is well defined for nodeless radial wave functions, such as $P_{4f}(r)$, and in other cases a simple interpolation may be used to prevent singularities in a plot of $V_{eff}(r)$.

For electrons in an open subshell, $V_{eff}(r)$ will be different for the different LS terms, resulting in term-dependent radial wave functions. We will shortly consider cases for which such variation among the terms is quite sizable; however, for many other cases, $V_{eff}(r)$ and $P_{n\ell}(r)$ are nearly the same for all terms of a configuration, and we may then employ a configuration-average Hartree-Fock (CAHF) method for which the direct potential and the exchange function are the same for all terms. When this is the case, it is possible to employ various approximations to the CAHF method, in which the Lagrangian multipliers, $E_{n\ell,n'\ell}$, are set to zero and the exchange function is replaced by some approximate, local exchange potential. The best known of these are the Hartree-Fock-Slater method,[11] in which the exchange function is replaced by Slater's free-electron gas exchange potential, and the modified HFS potential by Herman and Skillman.[12] In addition, there is the Hartree plus statistical exchange scheme[13] which incorporates an improved free-electron gas exchange potential and yields one-electron energies which agree quite well with those obtained from the CAHF method.

With today's high speed computers and improved numerical techniques, the HF or CAHF problem can be solved routinely and the various local approximations to the Hartree-Fock method are no longer widely used. However, most of the work done on wave function collapse in the neutral atoms was performed with one of these methods, and therefore they are included here. Furthermore, it is important to note that the HF equations are not solved in the form given in Eq. (2), but rather in their proper inhomogeneous form. The HF form of $V_{eff}(r)$ is used only as a descriptive device in explaining the nature of wave function collapse.

In hydrogen, the effective potential reduces to the form:

$$V_{eff}(r) = \frac{\ell(\ell+1)}{r^2} - \frac{2}{r} . \qquad (4)$$

With $\ell=3$, for f electrons, this is positive for $r<6$ (Bohr units), and beyond this there exists a shallow potential well with a mimimum at $r=12$. In multi-electron atoms, the core-electron wave functions do not extend appreciably into this outer region, and therefore, the potential for $r>6$ is nearly hydrogenic. However, for large Z, a second inner well develops at small radii where the effective nuclear charge is quite large. These two wells are separated by a positive centrifugal barrier, which if high enough, results in the existence of two quasi-independent sets of negative energy levels. Since the inner well is very narrow as compared to the outer hydrogenic region, the energy levels associated with this well are very widely spaced, and until Z becomes quite large, the lowest energy eigenvalue for the system is that of the outer well. Thus the binding energy for an f electron will be nearly equal to the hydrogenic value and $n^* \approx n$. As Z continues to increase, we reach a point where the inner well is sufficiently deep and wide that the inner-well level becomes the lowest one, and we then see an abrupt increase in the binding energy and an associated decrease in n^*.

The f-electron wave function has appreciable amplitude in only one of the two well regions, depending on whether the eigenvalue corresponds to an energy level of the inner or outer well. These two alternatives are shown in Fig. 2 for the 4f wave function in neutral $_{56}$Ba and $_{57}$La. The 4f wave function in Ba lies almost entirely in the outer-well hydrogenic region, the eigenvalue is nearly equal to that of hydrogen and $n^*=3.8$. However, in La the inner well is sufficiently deep and wide that the 4f wave function has collapsed completely into the

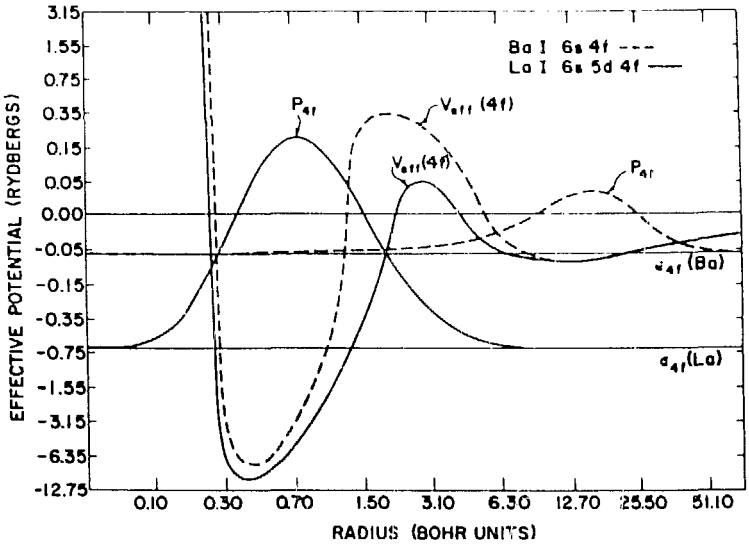

Fig. 2 Plot of the effective potentials and radial wave functions for the 4f electron in neutral Ba and La calculated using the HX approximation (Ref. 5). Nonlinear scales are used for both the effective potential and the radius. The radial wave functions are plotted on a linear scale the zero of which lies at the corresponding eigenvalue, noted in the figure by ε_{4f}.

inner-well region with a corresponding abrupt decrease in n^*.

At the same point where the 4f wave function collapses into the inner well, the first antinode for the 5f wave function moves abruptly from the outer region into the inner-well and barrier regions and becomes quite small in magnitude. This is illustrated in Fig. 3 where, in La, only the second antinode of the 5f wave function has any appreciable amplitude, and it lies in the outer-hydrogenic region where its shape resembles that of the 4f wave function in Ba. Thus the quantum defect ($n-n^*$) changes abruptly from a value close to zero to a value of nearly one in going from Z=56 to Z=57. More generally, if for a given atomic number the wave functions for the m lowest-lying nf subshells are in the inner well, then all excited nf wave functions have m antinodes with relatively small amplitudes in the inner-well or potential-barrier region, and therefore n-m-3 antinodes with much larger amplitudes in the outer-well, hydrogenic region. This implies an effective quantum number $n^* \approx n-m$, in agreement with the trends for f electrons shown in Fig. 1.

It is possible that an inner- and outer-well level might have equal energies. In such a case, the wave function would have large amplitudes in both wells and a minimum in the barrier region. For a fixed potential such as TF or TFD, such a situation will exist at some, in general non-integral, value of Z. However, for neutral atoms with an excited electron for which $\ell \geq 3$, where the barrier height is quite large, such a situation will be unstable when one uses a self-consistent-field model. If a small portion of charge is transferred from the outer to the inner well during the iterative process, the other electrons become more completely shielded from the nucleus and move to larger r; this in turn causes the excited electron to be less well shielded and it moves further toward the inner well; the inner well becomes deeper and wider and its level finally drops below the outer well level causing the excited electron to collapse completely into the inner region. This argument, which explains the

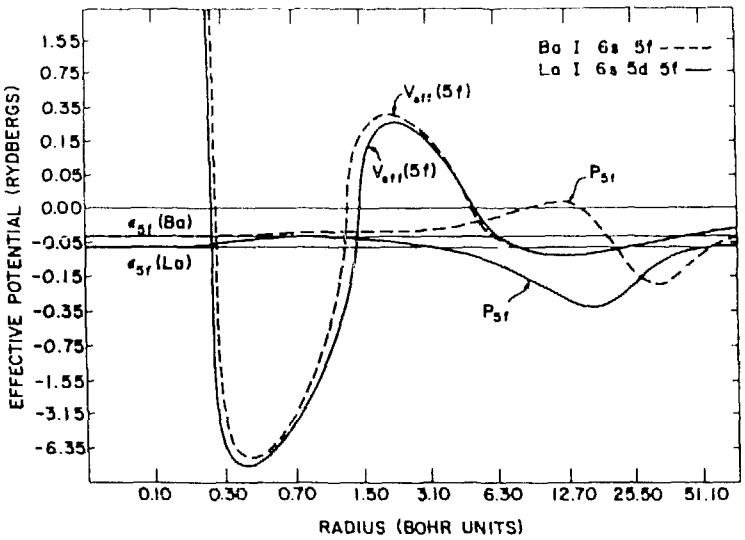

Fig. 3. Plot of the effective potentials and radial wave functions for the 5f electron in neutral Ba and La calculated using the HX approximation (Ref. 5). Further description is given under Fig. 2.

abrupt nature of the contraction for f electrons in neutral species, is valid only when the barrier height is large and we can correctly discuss two quasi-independent sets of energy levels. As we shall see, when the barrier height is small, there are cases where even a self-consistent procedure will yield appreciable amplitudes in each of the two regions.

Now let us consider the situation for d electrons. On the basis of the TF potential, Mayer[2] noted that double wells with positive potential barriers cannot occur for d electrons, and thus concluded that abrupt wave function and binding-energy changes should not occur for d electrons. However, Latter's subsequent calculations,[3] which employed both the TF and TFD potentials, corrected to have the proper $-2/r$ long range behavior, showed changes in energy similar to those for f electrons, although somewhat more gradual. Furthermore, Rau and Fano[4] pointed out that potential barriers do exist for d electrons when one uses a reasonably accurate potential, such as HFS with a tail cut-off at $-2/r$.[12]

The plot of effective quantum numbers for d electrons calculated using the HX potential is shown in Fig. 4. As can be seen, the changes in n^* with Z are still pronounced, although somewhat less abrupt than in the case of f electrons. The potential barriers for d electrons, when they do exist, are much more tenuous. For $\ell=2$, the hydrogenic well begins at r=3 and has its minimum at r=6. Thus, in a multi-electron atom, the core-electron wave functions will tend to overlap into the hydrogenic region, reducing the possibility of barrier formation. The barrier will be the most pronounced when the core electrons are the most compact, such as in the case of a closed-shell core like $K(3p^6 3d)$ where $\langle r\rangle_{3p}=1.43$.

The effective potentials and radial wave functions for the 3d electron in K and Ca are shown in Fig. 5. The effective potential for K does indeed have a well defined barrier region, although its maximum is actually below zero. The 3d wave function lies predominately in the

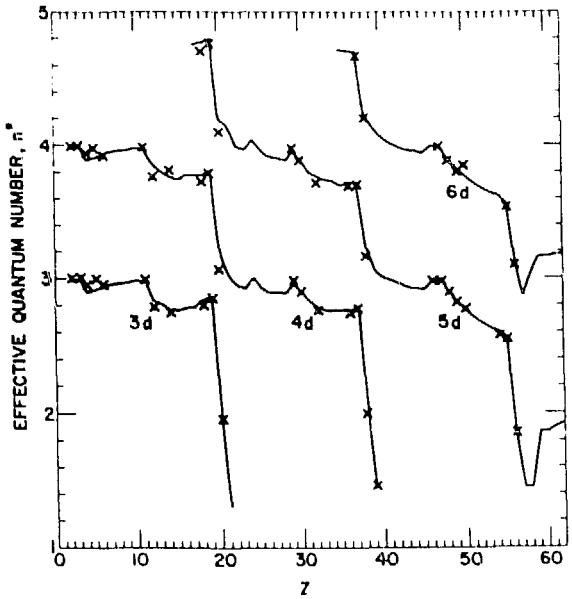

Fig. 4. Effective quantum numbers for d electrons as a function of atomic number from Ref. 5. The notation is the same as in Fig. 1.

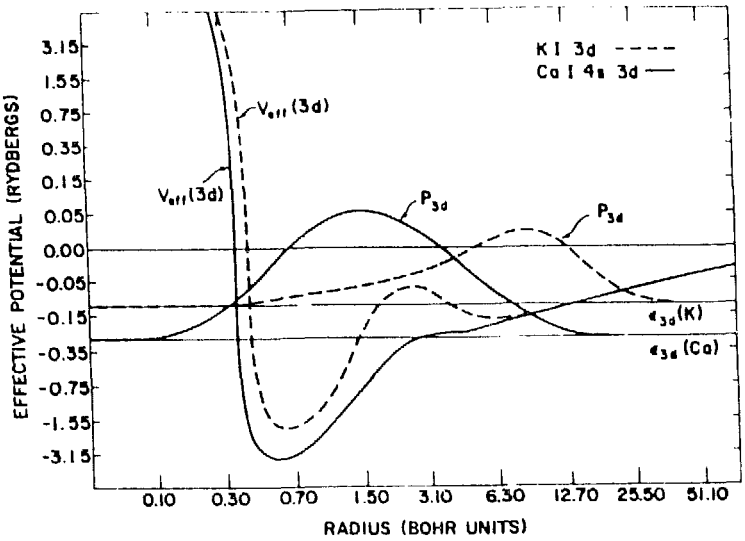

Fig. 5. Plot of the effective potentials and radial wave functions for the 3d electron in neutral K and Ca calculated using the HX approximation (Ref 5). Further description is given under Fig. 2.

outer well; however, it does have a noticeable overlap with the core region. In the next element Ca($3p^6 4s3d$), the 4s electron extends far into the outer-well region and provides very poor shielding for the added unit of nuclear charge. As a result, the barrier is wiped out, and the 3d wave function moves much further into the core region with the accompanying large change in n^* displayed in Fig. 4. The situation with the excited d electrons for which $n \geq 4$, is similar to that for the nf electrons already discussed, although again less dramatic.

Since the potential barriers for d-electron effective potentials are low in height, or not even present, the outer well regions are much less hydrogenic than they are for f electrons. This is the reason why, in Fig. 4, the n^* curves are not nearly as flat between drops, the values of n^* are not as close to integer values and the changes in n^* are not as close to unity as in the case of the f electrons shown in Fig. 1. This is especially true for high Z where the core-electron wave functions are less compact, and do not tend to provide the shielding necessary for the formation of well defined barriers. In general, the sudden variations in d-electron wave functions are much more a function of the detailed nature of the shell structure of the atom, and therefore much more sensitive to the core-electron configuration. Furthermore, predicted locations of d-wave function collapse within the periodic system are much more dependent on the central-field model employed.

All of the above discussion pertains only to neutral atoms; however, some of the more interesting physics associated with these centrifugal barrier effects occurs in ionized species. The effective potential for a multiply-ionized atom, can be written in the form:

$$V_{eff}(r) = \frac{\ell(\ell+1)}{r^2} - \frac{2Z_{eff}}{r} \qquad (5)$$

where Z_{eff} is the effective nuclear charge. For an excited electron which remains outside the core electrons in a Z-N ionized atom, Z_{eff}

reduces to the hydrogenic-like value Z-N+1, where N is the number of electrons. We see from Eq. (5) that the radius where the outer, hydrogenic-like well begins is inversely proportional to the value of the effective nuclear charge, and thus it decreases with ionization stage. Therefore, the core-electron wave functions, which have about the same radii in ions as in neutrals, have much larger overlaps with the outer well, even for $\ell \geq 3$. We then would expect much smaller barrier heights in ions, and these should decrease and become less important as a function of ionization stage.

In Fig. 6, we show the HX effective potential and radial wave function for the 4f electron in $Ba^+(5p^6 4f)$.[14] As can be seen, the effective potential is much less pronounced than in the case of neutral Ba shown in Fig. 2, and in fact, has a top which is negative. As a result, the 4f wave function is bimodal in shape with an appreciable amplitude in both the inner- and outer-well regions. Nevertheless, the largest portion of the amplitude of the wave function remains outside, and the quantum defect is relatively small (α.32).

As n increases, the barrier has gradually less effect on the nf wave functions, and their first antinodes penetrate deeper into the inner-well region.[15] This leads to some rather unusual properties in this nf Rydberg series. For example, the value of the quantum defect increases toward unity with increasing n,[5] more rapidly at first (for n=5, $n-n^*$=.65), and then very gradually, reaching a value of .85 by n=10. Such variations are so unusual that, for a time, they were suspected to be the result of misinterpretation of the observed spectra.[14,16] The behavior of these nf wave functions also leads to some unusual features in the absorption spectrum of Ba^+ from the long lived 5d ^2D states,[17] as discussed by Connerade.[15]

As we would expect from the above considerations, the d-electron

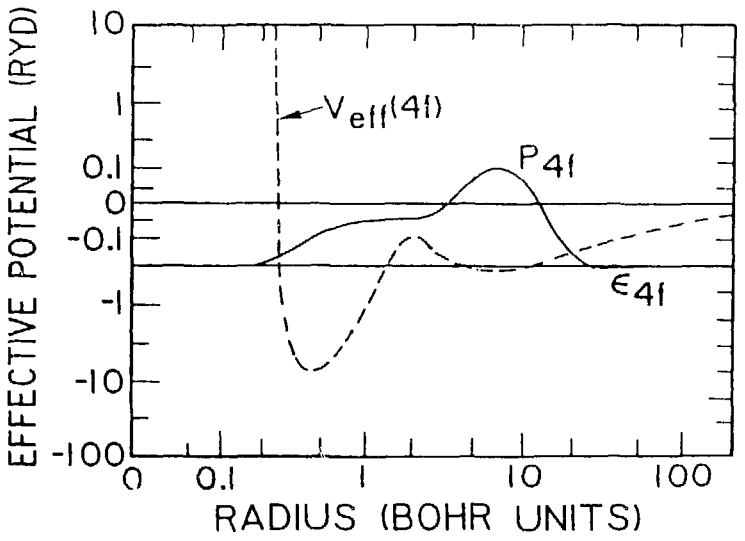

Fig. 6. Plot of the effective potential and radial wave function for the 4f electron in Ba^+ calculated using the HX approximation (Ref. 14). Further description is given under Fig. 2.

and f-electron orbitals collapse gradually as a function of ionization stage as compared to their variation as a function of Z for the neutral atoms. Nevertheless, these contractions can have important effects on the atomic structure of excited states involving d and f electrons. A discussion of the effects of such wave function variations for d electrons along isoelectronic sequences is given, for example, in Ref. 18. The contraction of f electrons as a function of ionization stage will be discussed in detail in the next section.

We now consider cases in which there is significant term dependence, or variation of the radial orbitals among the terms of a configuration. When this occurs, the CAHF method or the various local, configuration-average approximations mentioned in the last section no longer provide an accurate description for the system. Such term-dependent effects were first studied by the Hartrees[19] in a calculation of the 2s2p conf'guration, and a discussion of the results for the 2s2p ^3P and ^1P terms in Be is given by Fischer.[10] In this example, the 2s-2p exchange interaction in Be causes the 2p ^3P orbital to be slightly contracted ($\langle r\rangle$=2.9), while the 2p ^1P orbital is repelled to much larger radii ($\langle r\rangle$=5.0).[10]

These term-dependent effects are even more pronounced in configurations of the type p^5d near the beginning of the transition series, and d^9f near the beginning of the rare-earth series of elements. In order to understand this, we consider the energy expressions for the ^1P terms of these two configurations:

$$E(p^5d\ ^1P) = E_{ave}(p^5d) - 0.200F^2(pd) + 1.267G^1(pd) - 0.043G^3(pd) \quad (6)$$

$$E(d^9f\ ^1P) = E_{ave}(d^9f) - 0.229F^2(df) - 0.095F^4(df) + 1.957G^1(df) - 0.019G^3(df) - 0.021G^5(df), \quad (7)$$

where $F^k(\ell_i\ell_j)$ and $G^k(\ell_i\ell_j)$ are the Slater parameters for the direct and exchange electrostatic interactions, respectively; and the spin-orbit interaction terms are not included. The other terms of these configurations have coefficients for the electrostatic interactions of comparable magnitude, except for the coefficients of the dipole exchange integrals, G^1, which are small. Therefore, if we apply the variational principle to these energy expressions to obtain the term-dependent HF equations, the resulting exchange functions are quite different for the ^1P terms as compared to all other terms of the configuration; however, the potential terms and exchange functions for the other terms are well approximated by the CAHF method.

The large positive dipole exchange interactions within the expressions for $V_{eff}(r)$ of the ^1P terms can produce pronounced double-well effective potentials for the excited d and f electrons in such configurations. The sensitivity of the radial wavefunctions to these barriers may, in turn, lead to large term-dependent variations which have significant effects on a number of important atomic properties. Extensive calculations for configurations of the type p^5d have been performed by Hansen.[20] One of the most extreme examples of these effects for d^9f configurations occurs in the excited configuration $4d^95s^25p^66s^24f$ of neutral Ba. In Fig. 7 we show the 4f electron HF effective potentials and radial wave functions for this case.[21] The configuration average (CA) effective potential, which provides an accurate representation of the potential for the nine terms other than ^1P, has a very small barrier and a deep inner well. The large difference between this potential and that shown in Fig. 2 for the $4d^{10}5s^25p^66s4f$ configuration of Ba is due to the reduction in shielding when an electron is promoted from the closed 4d subshell to the 6s subshell. The CA 4f wave function has collapsed into

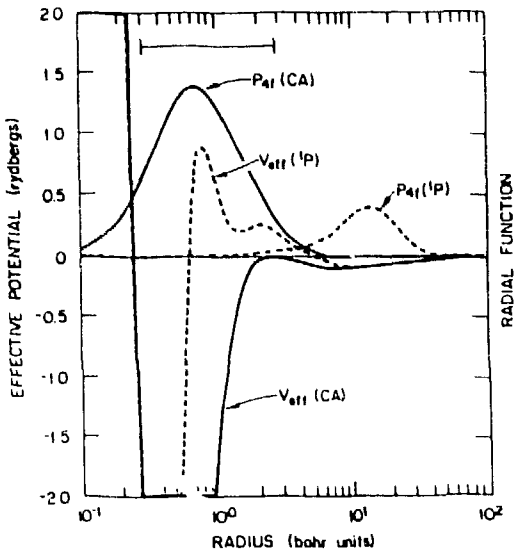

Fig. 7. Plot of the HF $4f_{CA}$ (solid curves) and 4f ^1P (dotted curves) effective potentials and radial wave functions for the the $4d^9 5s^2 5p^6 6s^2 4f$ configuration in neutral Ba (Ref. 21). A logarithmic scale is used for the radius. The bar indicates the range of radii over which the second antinode of the 4d radial wave function occurs.

the inner region, has a mean radius of 1.17 and a large overlap with the 4d electrons within the core. On the other hand, the ^1P effective potential has two distinct positive barriers; the large inner one is due to the positive exchange term, while the smaller outer one is due to the centrifugal term. However, contrary to the frozen-core term-dependent HF effective potential of Wendin and Starace,[22] the above potential, determined from a fully-relaxed, self-consistent HF calculation, does not go below zero in the region between the two barriers. These barriers cause the ^1P 4f wave function to remain in the outer-well region where it closely resembles a 4f hydrogenic wave function, has a mean radius of 17.5 and an extremely small overlap with the 4d radial wave function.

When one uses the $4f_{CA}$ wave function to calculate the position of the ^1P term it is found to lie above the $4d^9 5s^2 5p^6 6s^2$ ionization threshold because of the very large value of $G^1(4d,4f_{CA})$. However, as first pointed out by Hansen et. al.,[23] when one uses the proper 4f ^1P wave function, the $4d^9 4f$ ^1P term lies below the $4d^9$ ionization limit and has a binding energy close to that of a 4f hydrogenic electron.

Since all the nf ^1P wave functions in the $4d^9 5s^2 5p^6 6s^2 nf$ configurations of neutral Ba lie in the outer hydrogenic region, and thus have very small overlaps with the 4d wave function, the photo-absorption transitions $4d^{10} \rightarrow 4d^9 nf$ ^1P will have very little oscillator strength. The oscillator strength is, instead, transferred to the continuum transition $4d^{10} \rightarrow 4d^9 \varepsilon f$ ^1P, which is the cause of the well known giant resonance in the photoionization cross section of neutral Ba. This phenomenon will be discussed in detail by other authors in this volume, and therefore will not be pursued any further here.

In considering LS term dependence, it is important to note that one can approximate these effects by using CA radial wave functions and

performing a configuration-interaction calculation which includes the other members of the Rydberg series. For example, Younger[24] has performed such a calculation for $Xe^{8+}(4d^9 4f)$ and was able to approximate the term-dependent 4f ^1P wave function from an expansion of CA wave functions of the form:

$$P_{4f}(^1P) \cong c_1 P_{4f}(CA) + c_2 P_{5f}(CA) + c_3 P_{6f}(CA), \tag{8}$$

where c_1, c_2 and c_3 are the mixing coefficients in the configuration-interaction calculation. A similar calculation has been performed for $K^+(3p^3 3d\ ^1P)$,[14] but the Rydberg series members through n=11 had to be included before resonable agreement was obtained. Finally Wendin[25] and Wendin and Starace[22] have performed extensive CA, Rydberg series interaction calculations on the neutral Ba case just considered, in which very large basis sets had to be included.

By Brillouin's theorem,[26] configuration-interaction integrals which connect members of a Rydberg series, like the ones discussed above, will vanish when one uses the proper term-dependent HF wave functions. That is, correlations of the type represented by such interactions are already included in the zero-order, term-dependent wave functions. However, this is not true for CA wave functions. Nevertheless, if a complete set of CA wave functions are employed in a Rydberg series expansion, the resulting wave function must be identical to that obtained from the solution to the term-dependent HF equations. The primary advantage of the CA approach is that one can include LS term dependence and the effects of the spin-orbit interaction in a single multi-configuration calculation; the primary disadvantage is that many configurations may be required, including continuum states, before an accurate representation is obtained.

ELECTRON-IMPACT EXCITATION-AUTOIONIZATION

The study of electron-impact ionization increases our understanding of collisional dynamics and atomic structure and has important applications in laboratory and astrophysical plasmas. In the last decade, experimental and theoretical investigations have demonstrated the importance of the indirect mechanism involving the excitation of an inner-shell electron, followed by autoionization, to the total ionization process; in fact, for certain intermediate and heavy atomic sytems in lower stages of ionization, these indirect contributions can completely dominate the ionization cross section.[7,8,9]

The processes we wish to consider here are:

$$e + A^{q+} \rightarrow A^{(q+1)+} + e + e, \tag{9}$$

$$e + A^{q+} \rightarrow (A^{q+})^* + e \quad \hookrightarrow A^{(q+1)+} + e \tag{10}$$

where q is the charge of the atomic ion; Eq. (9) represents direct ionization, while Eq. (10) represents the excitation of an inner-shell electron to an intermediate state, followed by autoionization. The contribution of excitation-autoionization to the ionization cross section is given, to a very good approximation, by the the excitation cross section times a branching ratio for autoionization versus radiative stabilization. For relatively low stages of ionization, where the autoionizing rate is much higher than the radiative rate, this branching ratio is normally equal to unity, unless there are selection rules which inhibit

autoionization from a particular level.

When the first step in Eq. (10) involves an excitation of the form $d^{10} \rightarrow d^9f$, then the potential barrier effects and the resulting term dependence discussed in the last section become important in the determination of the size and shape of the ionization cross section. One of the best examples of this occurs in the Cd isoelectronic sequence.[27] Energy-level diagrams showing the $4d^{10}5s^2$ ground-state configurations and the excited $4d^95s^24f$ configurations for the Cd-like ions In^+, Sb^{3+}, and Xe^{6+} are given in Fig. 8. As can be seen, all of the 20 levels of $4d^95s^24f$ are autoionizing for the first two ions, while only the $4d^95s^24f$ $^1P_1$ level is above the ionization threshold in Xe^{6+}. The contribution of excitation-autoionization through the $4d^95s^24f$ configuration in In^+ is small. This can be understood by studying Fig. 9 where plots of the 4f effective potential and radial wave function for this ion are shown. The ^1P effective potential has both a large potential barrier and positive minimum in the inner well; as a result, the 4f ^1P wave function must remain in the outer well-region. However, the CA effective potential, which provides a fairly accurate representation for the other nine terms, has a much smaller barrier and the minimun in the inner well is now negative; nevertheless, the $4f_{CA}$ wave function still resides in the outer region, and is nearly identical to the 4f ^1P wave function. Thus the overlap of these wave functions with the 4d radial wave function is minimal, and the collision strength for the $4d^{10} \rightarrow 4d^94f$ electron impact excitation is extremely small.

As we move along the isoelectronic sequence, things begin to change, and by Sb^{3+}, term dependence sets in, as can be seen by examining Fig. 10. The increase in nuclear charge nearly wipes out the CA potential barrier, causing the $4f_{CA}$ wave function to drop into the inner region. However, the effective potential for the ^1P term still has

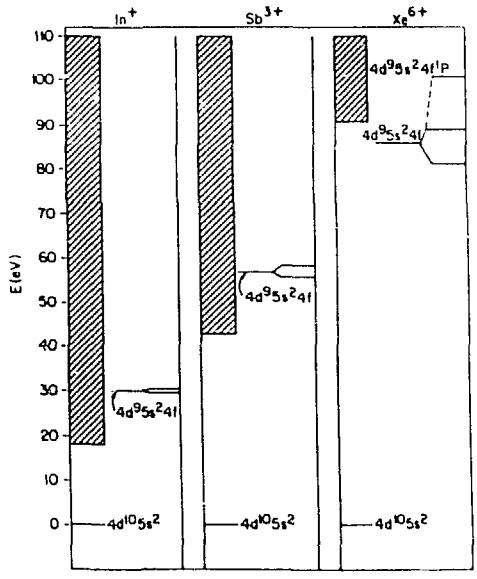

Fig. 8. Energy-level diagrams showing the $4d^{10}5s^2$ ground-state configurations, the $4d^95s^24f$ excited configurations and the ionization thresholds of In^+, Sb^{3+}, and Xe^{6+} (Ref. 27). Hatched regions indicate the ionization continuum for the next higher ionization stage.

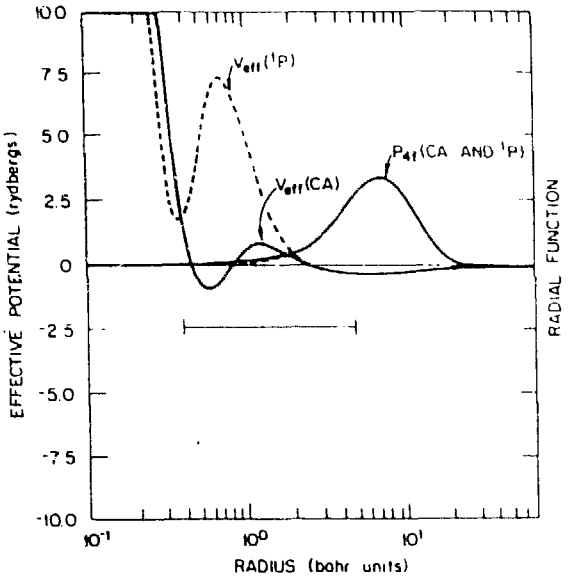

Fig. 9. Plots of the $4f_{CA}$ and 4f ^1P effective potentials and radial wave functions for the $4d^95s^24f$ configuration in In^+ (Ref. 27). The notation is the same as in Fig. 7.

a large positive barrier, which forces the 4f ^1P radial wave function to remain in the outer region. This has a pronounced effect on the size and shape of the $4d^{10}5s^2 \rightarrow 4d^95s^24f$ excitation cross section. The size of the dipole-allowed transition to the $^1P_1$ level depends on the overlap of the 4d and 4f ^1P wave functions which, in this ion, is quite small. However, the non-dipole excitations to the other 19 levels of $4d^95s^24f$ depend primarily on the size of the exchange contributions to the cross

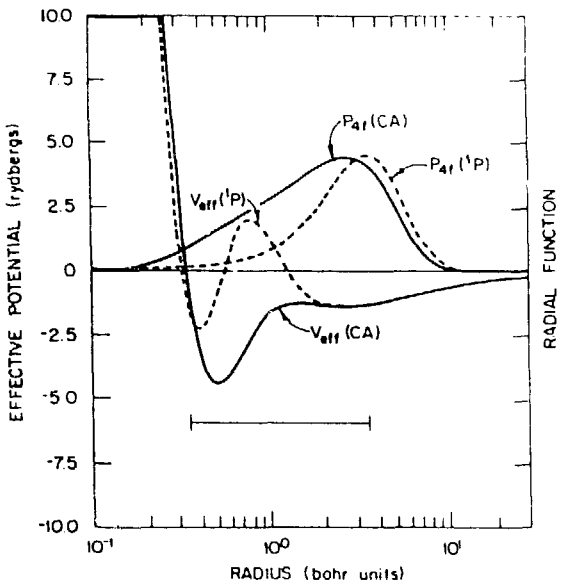

Fig 10. Plots of the $4f_{CA}$ and 4f ^1P effective potentials and radial wave function for the $4d^95s^24f$ configuration in Sb^{3+} (Ref. 27). The notation is the same as in Fig. 7.

section, and these contributions, are in turn, a function of the overlap of the 4d radial wave function with the outgoing scattered wave, as well as the overlap of the $4f_{CA}$ wave function with the incident wave. For electron energies near threshold, the incident wave has its first node in the barrier region, and thus there is a large overlap between its first antinode and the $4f_{CA}$ wave function which has a large amplitude in the inner-well region. However, as the energy increases, the first node of the incident wave moves further into the inner region and cancellation effects begin to decrease the magnitude of the collision strength. Therefore, in Sb^{3+} we would expect the excitation cross section for $4d^{10}5s^2 \rightarrow 4d^9 5s^2 4f$ to be dominated by the non-dipole transitions to the 19 levels other than $^1P_1$, and on the basis of the above discussion, its magnitude should fall off rapidly with electron energy.

The theoretical ionization cross section for Sb^{3+}, showing the excitation-autoionization contributions from both the $4d^9 5s^2 4f$ and $4d^9 5s^2 5f$ configurations is given in Fig. 11. The 5f configuration is also term dependent and the cross section is again dominated by the non-dipole transitions. The dipole collision strength has been transferred to higher members of the Rydberg series, and perhaps into the continuum. Thus, we would expect some of the dipole-allowed transitions to the $4d^9 5s^2 nf\ ^1P_1$ (n>5) levels to make measurable contributions to the ionization cross section, and they should be included in a complete calculation. These general conclusions are supported by a recent crossed electron-ion beam experiment performed on Sb^{3+} at ORNL[28], which shows a large indirect contribution to the ionization cross section of the shape shown in Fig. 11, but with apparent contributions from higher members of the Rydberg series. In addition, the experimental results show evidence for the added indirect process of resonant recombination followed by double autoionization,[29] which will not be discussed here. Finally, it should be mentioned that large non-dipole dominated excitation-autoionization contributions are also observed in several members of the Xe isonuclear sequence in low stages of ionization.[29]

Plots of effective potentials and radial wave functions for Xe^{6+}, the last ion in the Cd sequence to be considered, are shown in Fig. 12. The

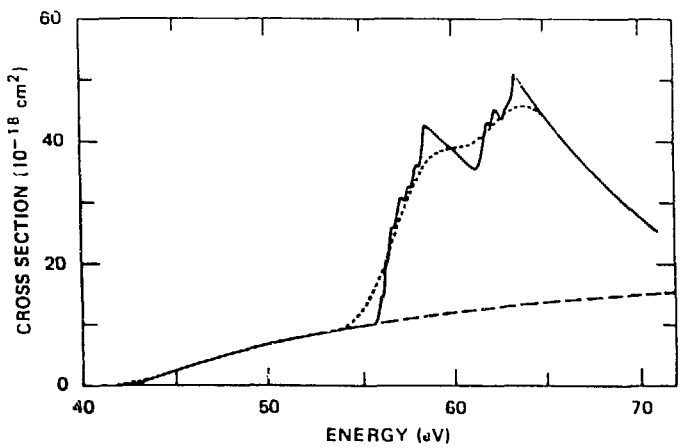

Fig. 11. Ionization cross section for Sb^{3+} (Ref. 27). Dashed curve, direct-ionization cross section calculated from the Lotz equation; solid curve, distorted-wave calculation of the indirect contribution due to $4d^{10}5s^2 \rightarrow 4d^9 5s^2 nf$ (n=4,5) plus Lotz; dotted curve, solid curve convoluted with a 2-eV Gaussian to simulate the experimental energy spread.

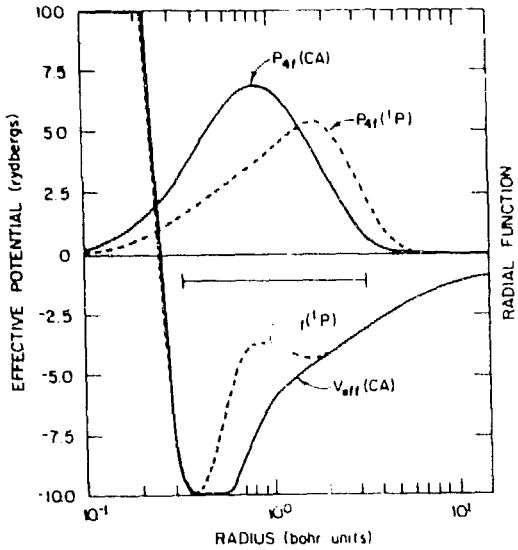

Fig. 12. Plots of the $4f_{CA}$ and 4f ^{1}P effective potentials and radial wave functions for the $4d^95s^24f$ configuration in Xe^{6+} (Ref. 27). The notation is the same as in Fig. 7.

additional increase in nuclear charge has caused the potential barrier for the ^{1}P effective potential to become negative and small, and the 4f ^{1}P wave function is on the verge of sliding completely into the inner-well region. For still higher stages of ionization the barrier will become completely insignificant, the 4f ^{1}P wave function will become indistinguishable from the $4f_{CA}$ wave function, and term-dependent effects will disappear. Nevertheless, for Xe^{6+}, these effects are still quite important and must be included in order to obtain accurate theoretical values of the ionization cross section. This is illustrated in Fig. 13, where we show the contribution of the $4d^{10}5s^2 \rightarrow 4d^95s^24f\ ^1P_1$ excitation followed by autoionization to the ionization cross section. It is legitimate to treat the only autoionizing level of the $4d^95s^24f$ configuration, $^1P_1$, separately since intermediate-coupling calculations indicate that it is over 99% pure. As can be seen, the distorted-wave calculations show a factor-of-2 reduction in the cross section when the proper 4f ^{1}P wave function, rather than the $4f_{CA}$ wave function is used. The very small difference between the term-dependent, distorted-wave results and the results one obtains when the 4f ^{1}P wave function is employed in a two-state, close-coupling calculation indicates that it is term dependence, and not continuum coupling, which is important for this case.

The more complete results for Xe^{6+} calculated using the distorted-wave method are shown in Fig. 14, along with the crossed electron-ion beam measurements of Gregory and Crandall.[30] The agreement between experiment and theory is quite good. The $4d^95s^24f\ ^1P_1$ level at 100.4 eV makes the largest contribution to the ionization cross section. However, the indirect contributions from other levels are also important. The step at 116.4 eV is due to the $4d^95s^25f\ ^1P_1$ level. The first antinode of the 5f ^{1}P wave function overlaps more strongly with the second antinode of the 4d wave function than does the first antinode of the $5f_{CA}$ wave function, which has moved further inside. This increases the cross section to the 5f $^1P_1$ level when the proper term-dependent radial wave function is used. Thus some of the 4f ^{1}P collision strength has been transferred to 5f ^{1}P. Also included in this calculation are the excitation-autoionization

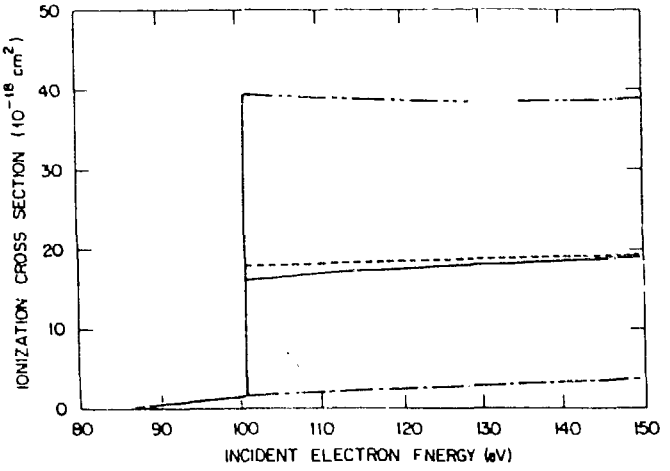

Fig. 13. Ionization cross section for Xe^{6+} showing the indirect contributions from the $4d^95s^24f\ ^1P_1$ level (Ref. 27). Dot-dash curve, direct-ionization cross section from the Lotz equation; solid curve, term-dependent, close-coupling calculation for the 4d → 4f $^1P_1$ excitation plus Lotz; dotted curve, term-dependent, distorted-wave calculation of the 4d → 4f $^1P_1$ excitation plus Lotz; chain curve, CA, distorted-wave calculation of the 4d → 4f $^1P_1$ excitation plus Lotz.

contributions from the $4d^95s^25d$ and $4d^95s^26p$ configurations, which show no term dependence. Finally, we include in Fig. 14 the excitation cross section to the lower levels of $4d^95s^24f$ (marked O for optical transitions) which are below the ionization threshold and, of course, do not contribute to the ionization cross section.

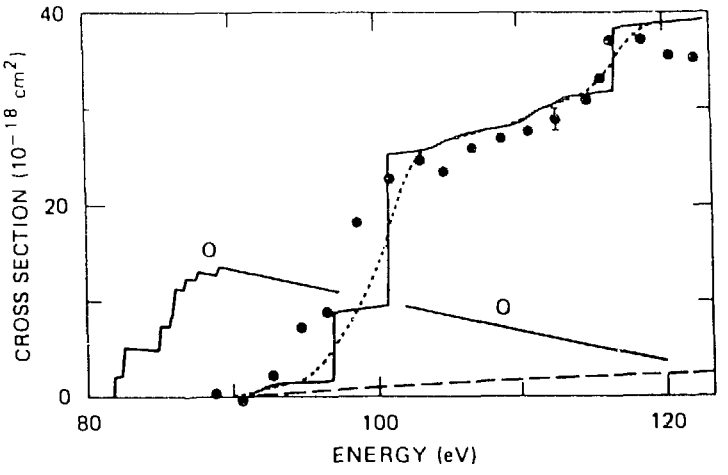

Fig. 14. Ionization cross section for Xe^{6+} (Ref. 27). Dashed curve, direct-ionization cross section calculated from the Lotz equation; solid curve, distorted-wave calculation of the excitations 4d → 4f,5f,5d,6p plus Lotz; dotted curve, solid curve convoluted with a 2-eV Gaussian to simulate the experimental energy spread; solid curve marked O is the total excitation cross section to non-autoionizing levels of $4d^95s^24f$; filled circles, experimental measurements, Ref. 30.

Potential-barrier and term-dependent effects can also be important for excitation-autoionization transitions involving excited d electrons near the beginning of the transition series of elements. This is especially true in transitions of the type:

$$e + np^6(n+1)s \longrightarrow np^5nd(n+1)s + e \quad \hookrightarrow np^6 + e \tag{11}$$

in the singly ionized species Ca^+, Sr^+, and Ba^+. These are the first ions where excitation-autoionization was found experimentally to dominate the total ionization cross section.[31,32,33] Hansen[34,35] first showed that the $np^5nd(n+1)s$ configurations in these ions exhibit pronounced term dependence, and he predicted that this would have a significant effect on the cross section for the $np^6 \longrightarrow np^5nd$ excitation. Since then, an R-matrix calculation[36] has demonstrated the importance of continuum coupling in this excitation process, and distorted-wave calculations[37] have confirmed Hansen's prediction regarding the significance of term dependence. However, to date, no calculation has been reported which includes both of these effects, and sizable disagreement between theory and experiment persists near the ionization threshold. Theoretical work on these ions, aimed at gaining a better understanding of the combined effects of term dependence and continuum coupling, is continuing.

DIRECT-IONIZATION CROSS SECTIONS

Potential-barrier and term-dependent effects in the continuum, which have been shown to be of great importance in certain photoionization transitions (see for example the review articles by Connerade[15] and Karaziya[38]), may also be significant in direct electron-impact ionization. Distorted-wave calculations have demonstrated that term dependence in the ejected-electron continuum can have a large effect on both the size and shape of single[39,40] and double electron-impact ionization cross sections.[41,42]

Let us first consider electron-impact ionization out of the 4d subshell within the Xe isonuclear sequence:[41,42]

$$e + Xe^{q+}(4d^{10}5s^25p^{6-q}) \longrightarrow Xe^{(q+1)+}(4d^95s^25p^{6-q}) + e + e, \tag{12}$$

where q is the ionization stage of the initial ion. For Xe^+, Xe^{2+}, and Xe^{3+}, all states of the configuration $4d^95s^25p^{6-q}$ are above the first ionization threshold, while for Xe^{4+}, only one third of the states of $4d^95s^25p^2$ are autoionizing. Thus for the first three ions, we would expect that ionization out of the 4d subshell should be followed by autoionization and contribute to the double-, rather than the single-, ionization cross section; in the case of Xe^{4+}, assuming a statistical distribution of the collision strength, about one third of the 4d ionization cross section will be observed as double ionization.

In all these ions, the 4d ionization is dominated by the $4d^9kf\ ^1P$ ejected-electron channel, and as one would expect from prior discussion, this channel is highly term dependent. In Fig. 15 we show the plots of the CA and ^1P effective potentials and continuum orbitals for Xe^+ and Xe^{2+} for an ejected-electron energy of 1 eV. For Xe^+ the CA effective potential has a small negative barrier, while the ^1P effective potential has large positive barrier. As a result, the first antinode of the kf_{CA} radial wave function is located in the inner-well region, where it has a large overlap with the second antinode of the 4d orbital; while the first anti-

node of kf ^1P is primarily in the outer-well region, where it overlaps only weakly with the second antinode of the 4d orbital. A strong overlap between the kf ^1P orbital and the 4d orbital will not occur until we reach higher ejected-electron energies. For Xe^{2+}, at the same ejected-electron energy, the situation is quite different. With the decreased shielding resulting from the removal of another 5p electron, the barrier in the CA effective potential has disappeared and the kf_{CA} has moved far enough into the inner region that wave cancellation has begun to decrease its overlap with the 4d wave function. However, the decrease in the ^1P potential barrier has caused the kf ^1P continuum orbital to slide much further into the inner region, where it has a sizable overlap with the second antinode of the 4d wave function.

On the basis of these simple effective-potential arguments, we can make a number of predictions regarding the 4d ionization cross section for these two ions. In Xe^+, the use of the proper term-dependent orbital, rather than the configuration-average orbital, for the kf ^1P ejected-electron channel should lead to a reduction of the cross section near threshold (i.e., a delayed onset) and, most likely, an overall decrease in the magnitude of the cross section. However, in the case of Xe^{2+}, the 4d ionization cross section calculated with the term-dependent continuum function should be larger than that calculated with the CA orbital, even near threshold.

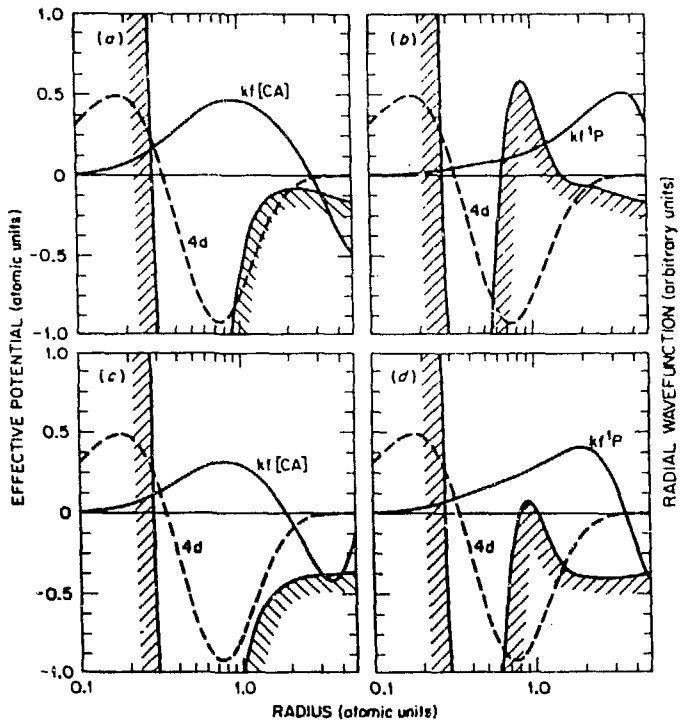

Fig. 15 CA and ^1P term-dependent effective potentials and radial wave functions for the f continuum electron ejected from the 4d subshell in Xe^+, (a) and (b), and Xe^{2+}, (c) and (d) (Ref. 42). Hatched solid curves, effective potentials; solid curves, kf continuum wave functions at an energy of 1 eV; dashed curves, 4d bound orbital. Note here that the effective potentials are in hartree atomic units, rather than rydbergs.

The experimental and theoretical results for double ionization in Xe^{+} through Xe^{4+} are shown in Fig. 16. The direct double-ionization cross section was estimated from the binary-encounter approximation of Gryzinski,[43] and as expected, it decreases rapidly with ionization stage. The 4d ionization-autoionization contributions, however, dominate the total double-ionization cross section for all 4 ions, and show significant term-dependent effects. The calculations which employ the kf ^1P term-dependent continuum functions for the $4d^9kf\ ^1P$ ejected-electron channel also include an estimate for the effects of ground-state correlation by incorporating the important $4d^{10} \longleftrightarrow 4d^8 4f^2$ configuration interaction. The difference between the CA and the term-dependent results for Xe^{+} and Xe^{2+} is about as expected from the potential-well arguments above and, in each case, the term-dependent results are closer to the experimental measurements.[44] The results for Xe^{3+} are similar to those for Xe^{2+}; however, in all three ions the experimental threshold is below that predicted by theory. In the case of Xe^{4+}, we also show curves for the 4d ionization cross sections multiplied by the fraction of states of the configuration $4d^9 5s^2 5p^2$ which autoionize (1/3). From a comparison of these scaled curves with the experimental measurements, it would appear that the collision strength is not distributed statistically.

Recently Younger[40] completed a theoretical study of photoionization and direct electron-impact ionization out of the 4d subshell for ten ions

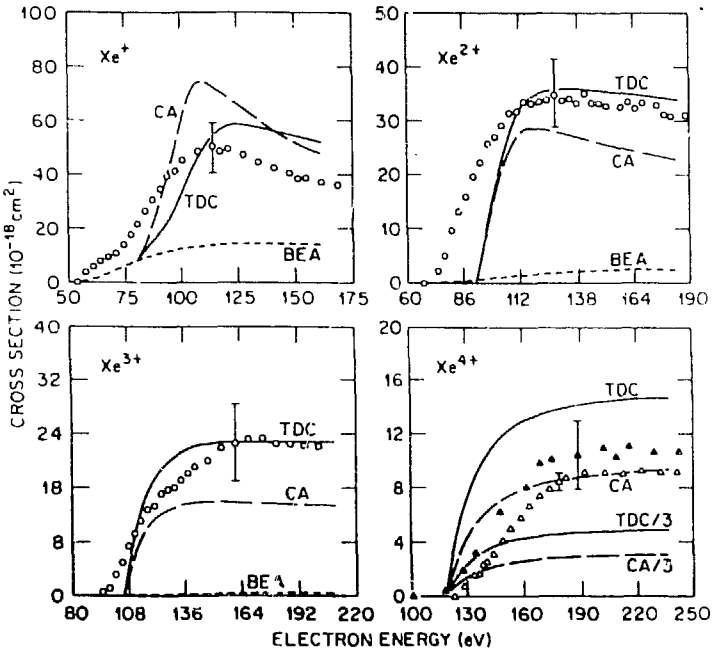

Fig. 16. Electron-impact double-ionization cross sections for (a) Xe^{+}, (b) Xe^{2+}, (c) Xe^{3+}, and (d) Xe^{4+}. Open circles and darkened triangles, experimental data (Ref 44); open triangles, experimental data (Ref 42); short-dashed curves labeled BEA, direct-double ionization using the binary-encounter approximation; long-dashed curve labeled CA, 4d ionization contribution using configuration-average kf radial wave functions plus direct-double ionization; solid curves labeled TDC, 4d ionization contribution using kf ^1P term-dependent radial wave functions with ground-state correlations plus direct-double ionization.

within the palladium isoelectronic sequence, with ground-state configurations $4d^{10}$. The cross sections are, as in the cases discussed above, dominated by the $4d^9kf$ ^1P channel, and term dependence was found to be significant up to a charge state of +10. In an earlier calculation,[45] he demonstrated similar effects for electron-impact ionization out of the closed 5d subshell in Hg^+.

Term dependence in the ejected-electron continuum may also be important in electron-impact ionization out of closed p subshells. This was shown in a study of the argon isoelectronic sequence[39] where, for low stages of ionization, the 3p ionization cross section is dominated by the $3p^5kd$ ^1P ejected-electron channel. In neutral argon, the term-dependent effective potential for the d continuum electron differs significantly from the CA effective potential and has a well defined barrier region. Thus at low ejected-electron energies, the kd ^1P partial wave, unlike the kd_{CA} wave, will not penetrate the barrier and will have a small overlap with the 3p orbital; however, at some higher ejected-electron energy the penetration will become appreciable. This behaviour, which is similar to that already discussed for the kf ^1P wave in Xe^+, is displayed in Fig. 17 where the phase shift, δ, is plotted as a function of ejected-electron energy for the CA and term-dependent kd partial waves. The phase shift for the kd_{CA} wave is large at very low energies, while the kd ^1P phase shift is quite small until the wave begins to penetrate the barrier at about 4 eV.

The ionization cross section for Ar I calculated using the CA and term-dependent kd partial wave for the $3p^5kd$ ^1P ejected-electron channel are shown in Fig. 18. As can be seen, term-dependence is quite important for electron energies up to more than three times threshold. Also shown is a term-dependent calculation corrected for the effects of ground-state pair correlation $3p^6 \longleftrightarrow 3p^43d^2$. Term-dependence enhances the influence of this interaction by increasing the overlap of the kd continuum wave and the 3d correlation orbital.[39] For the higher members

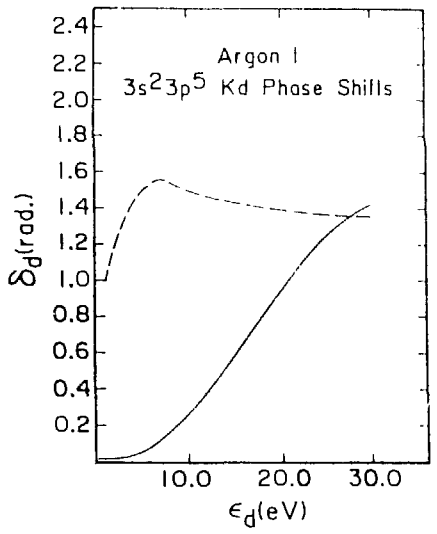

Fig. 17. Phase shifts, δ_d, for the kd partial waves in neutral argon as a function of ejected-electron energy, ε_d (Ref. 39). Dashed curve, from a distorted-wave calculation using the CA effective potential; solid curve, distorted-wave calculation using the ^1P effective potential.

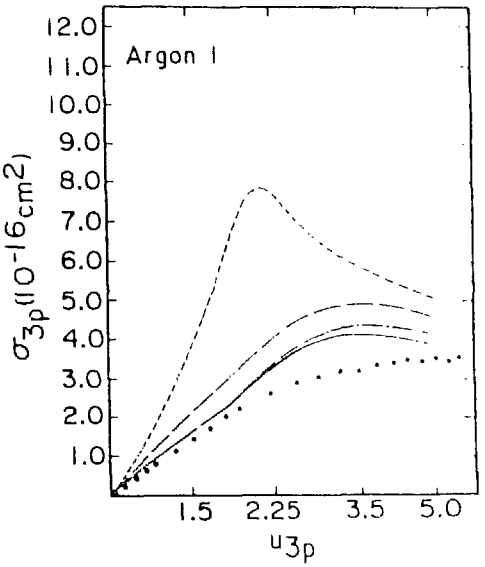

Fig. 18. 3p electron-impact ionization cross section, σ_{3p}, of neutral argon (Ref. 39). The incident electron energy in threshhold units is represented by u_{3p}. Short dash, calculated using the CA kd wave for the $3p^5kd\ ^1P$ ejected-electron channel; long dash, calculated using the term-dependent kd wave for the $3p^5kd\ ^1P$ ejected-electron channel; solid curve; term-dependent calculation with approximate ground-state correlation; dot-dash, solid curve plus 3s subshell ionization; open circles, experimental measurements (Ref. 46).

of this isoelectronic sequence the effects of term dependence decrease rapidly with ionization stage. Not only is the barrier height diminished, reducing the difference between the kd_{CA} and kd ^1P partial waves, but also, the relative importance of the kd ^1P exit channel to the total ionization cross section decreases.[39]

CONCLUSIONS

The sudden changes with atomic number in the binding energy of excited d and f electrons preceding the onset of transition and rare-earth series of elements can be explained in terms of one-electron effective potentials. The change in binding energy and the associated wave function collapse are most abrupt when the potential contains a centrifugal barrier which is positive and well defined. Thus the contraction of wave functions is more gradual for d electrons than for f electrons and occurs much less abruptly for ionized species than for neutrals.

Barriers in the effective potential for configurations of the type p^5d and d^9f are enhanced by an unusually large positive exchange interaction for the ^1P terms. This may lead to a large difference between the ^1P Hartree-Fock radial wave functions and the wave functions for all other terms of these configurations, especially near the beginning of the transition and rare-earth series of elements, where the collapse of the wave function is about to occur. This term dependence can have a significant influence on many atomic properties, including the excitation and ionization of both neutral and ionized species.

ACKNOWLEDGEMENTS

The authors would like to thank C. Bottcher and S. Younger for a number of very useful discussions. The collaborative efforts of the electron-ion beam experimental groups at ORNL and JILA are gratefully acknowledged. This work was supported by the Office of Fusion Energy, U. S. Department of Energy, under Contract No. DE-AC05-84OR21400 with Martin Marietta Energy Systems, Inc., and under Contract No. DE-FG05-86ER53127 with Auburn University.

REFERENCES

1. E. Fermi, in: "Quantentheorie und Chemie," H. Falkenhagen, ed., S. Hinzel-Verlag, Leipzig, 1928, p. 95.
2. M. Mayer, Phys. Rev. 60, 184 (1941).
3. R. Latter, Phys. Rev. 99, 510 (1955).
4. A. R. P. Rau and U. Fano, Phys. Rev. 167, 7 (1968).
5. D. C. Griffin, K. L. Andrew, and R. D. Cowan, Phys. Rev. 177, 62 (1969).
6. D. C. Griffin, R. D. Cowan, and K. L. Andrew, Phys. Rev. A 3, 1233 (1971).
7. R. A. Falk, G. H. Dunn, D. C. Griffin, C. Bottcher, D. C. Gregory, D. H. Crandall, and M. S. Pindzola, Phys. Rev. Lett. 47, 494 (1981).
8. D. C. Griffin, C. Bottcher, and M. S. Pindzola, Phys. Rev. A 25, 1374 (1982).
9. C. Bottcher, D. C. Griffin, and M. S. Pindzola, J. Phys. B 16, L65 (1983).
10. C. Froese Fischer, "The Hartree-Fock Method for Atoms," Wiley, New York (1977).
11. J. C. Slater, Phys. Rev. 81, 385 (1951).
12. F. Herman and S. Skillman, "Atomic Structure Calculations," Prentice-Hall, Inc., Englewood Cliffs, New Jersey (1963).
13. R. D. Cowan, Phys. Rev. 163, 54 (1967).
14. R. D. Cowan, "The Theory of Atomic Structure and Spectra," University of California Press, Berkeley (1981).
15. J. P. Connerade, Contemp. Phys. 19, 415 (1978).
16. V. Kaufman and J. Sugar, J. Res. Natl. Bur. Stand. 71A, 583 (1967).
17. R. A. Roig and G. Tondello, J. Opt. Soc. Am. 65, 829 (1975).
18. R. D. Cowan, J. Opt. Soc. Am. 58, 924 (1968).
19. D. H. Hartree and W. Hartree, Proc. Roy. Soc. A154, 588 (1936).
20. J. E. Hansen, J. Phys. B. 5, 1083 (1972).
21. D. C. Griffin and M. S. Pindzola, Comments At. Mol. Phys. 13, 1 (1983).
22. G. Wendin and A. F. Starace, J. Phys. B 11, 4119 (1978).
23. J. E. Hansen, A. W. Fliflet, and H. P. Kelly, J. Phys. B 8, L127 (1975).
24. S. M. Younger, Phys. Rev. A 22, 2682 (1980).
25. G. Wendin, J. Phys. B 9, L297 (1976).
26. L. Brillouin, J. Phys. Radium 3, 373 (1932).
27. M. S. Pindzola, D. C. Griffin, and C. Bottcher, Phys. Rev. A 27, 2331 (1983).
28. D. C. Gregory and A. M. Howald, Phys. Rev. A 34 (1986).
29. D. C. Griffin, C. Bottcher, M. S. Pindzola, S. M. Younger, D. C. Gregory, and D. H. Crandall, Phys. Rev. A 29, 1729 (1984).
30. D. C. Gregory and D. H. Crandall, Phys. Rev. A 27, 2338 (1983).
31. B. Pert and K. T. Dolder, J. Phys. B 1, 872 (1968).
32. B. Pert, J. G. Stevenson, and K. T. Dolder, J. Phys. B 6, 146 (1973).
33. B. Pert and K. T. Dolder, J. Phys. B 8, 56 (1975).
34. J. E. Hansen, J. Phys. B 7, 1902 (1974).

35. J. E. Hansen, J. Phys. B 8, 2759 (1975).
36. P. G. Burke, A. E. Kingston, and A. Thompson, J. Phys. B 16, L385 (1983).
37. D. C. Griffin, M. S. Pindzola, and C. Bottcher, J. Phys. B 17, 3183 (1984).
38. R. I. Karaziya, Sov. Phys. Usp. 24, 775 (1981).
39. S. M. Younger, Phys. Rev. A 26, 3177 (1982).
40. S. M. Younger, Submitted Phys. Rev. A (1986).
41. M. S. Pindzola, D. C. Griffin, and C. Bottcher, J. Phys. B 16, L355 (1983).
42. M. S. Pindzola, D. C. Griffin, C. Bottcher, D. H. Crandall, R. A. Phaneuf, and D. C. Gregory, Phys. Rev. A. 29, 1749 (1984).
43. M. Gryzinski, Phy. Rev. 138, A336 (1965).
44. C. Achenbach, A. Muller, E. Salzborn, and R. Becker, Phys. Rev. Lett. 50, 2070 (1983).
45. S. M. Younger, private communication.
46. R. K. Asuni and M. V. Kurepa, J. Electron. Control 15, 41 (1963).

DISCLAIMER

This report was prepared as an account of work sponsored by an agency of the United States Government. Neither the United States Government nor any agency thereof, nor any of their employees, makes any warranty, express or implied, or assumes any legal liability or responsibility for the accuracy, completeness, or usefulness of any information, apparatus, product, or process disclosed, or represents that its use would not infringe privately owned rights. Reference herein to any specific commercial product, process, or service by trade name, trademark, manufacturer, or otherwise does not necessarily constitute or imply its endorsement, recommendation, or favoring by the United States Government or any agency thereof. The views and opinions of authors expressed herein do not necessarily state or reflect those of the United States Government or any agency thereof.